Effect of rehabilitation exercise durations on the dynamic bone-repair process by coupling polymer scaffold degradation and bone formation

Quan Shi[1], Qiang Chen[1,*], Nicola Pugno[2,3,4], Zhi-Yong Li[1,5,*]

[1]Biomechanics Laboratory, School of Biological Science & Medical Engineering, Southeast University, 210096 Nanjing, PR China

[2]Laboratory of Bio-Inspired & Graphene Nanomechanics, Department of Civil, Environmental and Mechanical Engineering, University of Trento, I-38123 Trento, Italy

[3]School of Engineering and Materials Science, Queen Mary University of London, Mile End Road E14NS London, UK

[4]Ket Lab, Edoardo Amaldi Foundation, Italian Space Agency, Via del Politecnico snc, 00133 Rome, Italy

[5]School of Chemistry, Physics and Mechanical Engineering, Queensland University of Technology(QUT), QLD 4001 Brisbane, Australia

Revised Manuscript submitted to Biomechanics and Modeling in Mechanobiology

[*]Corresponding Authors:

Associate Prof. Dr. Qiang Chen

Email: chenq999@gmail.com

Prof. Dr. Zhi-Yong Li

Email: zylicam@gmail.com

Tel./Fax: +862583792620

Abstract

Bone disorders are common, and the implantation of biodegradable scaffold is considered as a promising method to treat the disorders, but the knowledge of the dynamic mechanical process of the scaffold-bone system is extremely limited. In this study, based on the representative volume cell (RVC) of a periodic scaffold, the influence of rehabilitation exercise duration per day on the bone repair was investigated by a computational framework. The framework coupled the polymer scaffold degradation and the bone remodeling. The scaffold degradation was described by a function of stochastic hydrolysis independent of the mechanical stimulation, and the bone formation was remodeled by a function of the mechanical stimulation, *i.e.*, strain energy density (SED). Then, numerical simulations were performed to study the dynamic bone repair process. The results showed that the scaffold degradation and bone formation in the process were competitive. The longer the exercise duration per day was, the earlier the bone matured and the lower the final Young's modulus, but all exercise durations promoted the bone maturation with a final Young's modulus around 1.9±0.3 GPa. This indicates that the longer exercise duration could accelerate the bone-repair process but not improve the bone stiffness. The present study is helpful to understand and monitor the bone repair process, and useful for the bone scaffold design in bone tissue engineering.

Keywords: Bone repair, Rehabilitation exercise duration, Scaffold degradation, Bone remodeling, Finite element model (FEM).

1. INTRODUCTION

Bone scaffolds used to repair bone disorders are in increasing need, since the disorders are of great concern due to the increasing aging population. According to the statistics, millions of orthopaedic procedures are worldwide performed every year [1]. Successful bone tissue regeneration or repair requires a porous scaffold, which should possess suitable porous structure, mechanical property, biocompatibility, biodegradability, and osteoinduction ability, etc. From the biomechanical point of view, the mechanical properties of scaffolds should mimic those of natural bones. In particular, the degradation rate of scaffolds and the formation rate of bones should match each other in the repair process, and this is well-accepted as a gold standard in the bone tissue engineering [2-4]. Otherwise, a stiff scaffold induces the well-known "stress shielding" effect, and a soft scaffold cannot maintain a porous structure in the load-bearing tissue regeneration. Moreover, it is reported that physical exercise is beneficial to the bone repair [5], but to the best knowledge of authors, the effect of physical exercise durations on the bone repair has not been quantified. Therefore, studying the scaffold-degradation/bone-formation dynamic coupling process and the influence of rehabilitation exercise durations on the process is very necessary.

Biodegradable polymer scaffolds show promise because of their absorbable property, adequate mechanical property and controllable degradation rate [6], and the polymer degradation can create extra space allowing new bone in-growth to replace the scaffold eventually. Polymer degradation is due to the scission of long molecular chains caused by hydrolytic reactions and others, and it results in a low molecular weight and mass loss of the polymer. Finally, the polymer’s structure and physical properties change. At present, there are two erosion mechanisms to describe the polymer degradation. One is surface erosion, namely, as the surface is eroded, the erosion front moves toward the material core [7]; the other is bulk erosion, namely, erosion simultaneously occurs throughout the material. Most numerical analyses of polymer degradation consider the bulk erosion. For example, Gopferich [8, 9] theoretically described bulk erosion by considering a stochastic hydrolysis process. Chen et al. [10] proposed a hybrid mathematical model that combined stochastic hydrolysis and diffusion-governed autocatalysis to simulate bulk-erosive biodegradable devices, which showed an excellent agreement with experimental data in literature. However, in reality, the surface and bulk erosion usually co-exist or compete [11,12].

Bone tissue growth is under constant and complex remodelling. The remodeling phenomenon can be generally described by the well-known Wolff's law, and it states that the mechanical stimulus plays an important role in the remodeling processes [13-16]. Based on the concept, researchers developed different bone remodeling theories by applying different mechanical parameters, such as strain, stress or strain energy density. For example, Cowin and Hegedus [17] firstly proposed a dynamic theory of the cortical bone remodeling, which assumed that the remodeling rate was a linear function of the strain, and trabecula self-adaptably changed till an equilibrium strain state was reached. Carter et al. [18, 19] introduced a ‘self-optimization’ algorithm based on the strain energy density (SED), which assumed that the mechanical stimulus was proportional to the effective stress field. Later, Huiskes et al. [15] simplified the algorithm by considering SED rate for the bone remodeling. Adachi et al. [20] used strain gradient and developed a theory that bone formed when the stress of an element was less than the contribution from its neighboring elements, instead, bone was absorbed.

The above introduces the scaffold degradation and bone remodeling, respectively. Regarding the coupling model, Adachi et al [21] and Chen et al. [22] combined the hydrolysis-based scaffold degradation theories and bone remodeling theories, and developed two scaffold degradation/bone formation coupling models to optimize periodic scaffold architectures, and both showed that different structures had different influences on the coupling process. It is worth mentioning that Chen et al. [22] also introduced the auto-catalytic effect, the homogenization technique, and topology optimization into the finite element model to find an optimal scaffold structure. However, both degradation models were based on the bulk erosion, and did not consider how rehabilitation exercise durations affected the bone repair either.

In the sense of experiments, it is hard to quantitatively investigate the coupling process. Finite element (FE) analysis as an effective method is often employed to study the relevant issues. It not only provides information about the changes of biomechanical environments after scaffold implantation, but also flexibly incorporates mathematical models for the coupling dynamic process, allowing pre-evaluation on how scaffold impacts on the bone repair and further optimal design of the scaffolds.

This study aims to develop a theoretical method to study the influence of the rehabilitation exercise duration per day on the bone repair. First, the scaffold degradation including both bulk and surface erosions is modeled by a stochastic function, and thee degradation is unrelated to the mechanical stimulus. Different from the degradation, the bone remodeling involving bone resorption and formation is mathematically formulated in terms of SED. Then, by utilizing the FE method and considering different rehabilitation exercise durations per day, the two processes are coupled to study the bone-repair process within 200 days after scaffold implantation.

2. METHODS

2.1. Numerical implementation

Geometry – A porous periodic scaffold was investigated, as seen in Figure 1a. Due to the scaffold periodicity, the coupling model of the scaffold degradation and bone formation was formulated based on the scaffold RVC, as seen in Figure 1b. The RVC was obtained by subtracting three orthotropic and concentric cuboids with identical size 1000μm × 600μm × 600μm from a cube with side length 1000μm. The porosity of the RVC (or scaffold) was calculated as 64.8%, which located in the range of the porosity of bones (5%-90% [23]).

Materials – After scaffold implantation, the pores are usually occupied by a fluid. Interstitial fluid (ISF) was observed to mediate signal transduction in mechanical loading-induced remodeling [24], thus, the porous part of the RVC here was assumed to be initially occupied by the ISF. All materials (scaffold, bone and ISF) in the RVC, were assumed to be isotropic and linear-elastic solids, and the ISF was nearly incompressible. The scaffold and bone shared the same Poisson's ratio, which was a constant in the entire degradation-remodeling process.

Boundary conditions – The RVC bottom surface was fixed, and a rigid plate was placed on the RVC top surface to ensure that the RVC was uniaxially and uniformly deformed in the z-direction. The loading history was a trapezoidal pulse with a period 1 day, and it included relax, ascending, holding, and descending stages. The relax stage t_{relax} meant no exercise, while the rest three stages t_{exercise} described the exercise duration in a day. The cancellous bone is generally subjected to a compressive stress in a range of 0.5–10 MPa [22, 25], and as suggested by Shefelbine et al. [26], we here used 3 MPa, as seen in Figure 2a. It is worth mentioning that the ascending/descending stages in the loading history were set to be 0.05 day to avoid the abrupt change of the loading history between the relax and holding stages, which might result in an inaccurate simulation. Seven exercise durations denoted by duty-cycles (*i.e.* $t_{\mathrm{exercise}}/(t_{\mathrm{exercise}}+t_{\mathrm{relax}})$) from 0.2 to 0.8 with 0.1 interval, were studied. In the seven cases, degraded scaffold and formed bone were assumed not to fracture.

RVC mesh and simulation – The RVC was meshed into 8000 (20 × 20 × 20) identical voxel finite elements with side length l=50μm, Figure 2b. The simulation of the scaffold degradation and bone formation was performed by coding the user subroutine (VUMAT) of the commercial software Abaqus/Explicit (DS SIMULIA, USA), and the element type was the reduced-integration element C3D8R. To display the states of materials assigned to each element during the process, we defined a "state field" χ, namely, if χ= 1, the element was scaffold, if χ= 2, the element was bone (including unmatured and matured), and the element was ISF when χ= 3.

2.2. Polymer scaffold degradation

Polylactic acid (PLA) was taken as the constituent material of the scaffold, which is a kind of saturated aliphatic polyesters. In the degradation model, two judgments were used to denote the complete degradation of the scaffold elements. One was based on the polymer molecular weight, which was influenced by both 'bulk' and 'surface' erosions; the other was based on a modified stochastic degradation algorithm, which was commonly used to describe the hydrolytic degradation of polymers. The two judgments are stated as follows:

Polymer molecular weight: The number average molecular weight M_n of the scaffold element decreases in the degradation, and $\beta(t)$ is used to describe the degree of degradation, which is the ratio of the number average molecular weight $M_n(t)$ of scaffold elements at time t to the weight M_{n-nd} of the ideal non-degraded scaffold element, i.e.,

$$\beta(t) = \frac{M_n(t)}{M_{n-nd}} \tag{1}$$

When M_n(t) reduced to a threshold, the scaffold did not have mechanical properties any more.

This corresponded to $\beta(t)$ decreasing from 1 to a threshold, and indicated that the scaffold changed into the ISF. Moreover, because $M_n(t)$ resulted from the random breakage of polymer chains in the hydrolytic and autocatalytic reactions, the exponential pseudo first-order kinetics was used to describe the bulk erosion as [10]:

$$\beta(t) = e^{-\kappa_1 t} \tag{2}$$

where e is the base of the natural logarithm, κ_1 is the bulk degradation rate constant with dimension of s^{-1}, which is determined by material properties and scaffold morphology, etc. In the ideal case, the polymer at initial stage was non-degraded, and $M_n(0)=M_{n\text{-}nd}$ held for all scaffold elements. However, in reality, randomly initial degradation by hydrolysis often occurs in all scaffold elements before implantation, thus, each element had a randomly assigned initial porosity α=1-$\beta(0)$ [10], which resulted in a initial molecular weights $M_n(0)=(1-\alpha)M_{n\text{-}nd}$. Regarding the initial porosity, it was often studied in the drug release kinetics of polymers, and varied from 0.2 to 0.7 [27, 28]. Here, the upper limit 0.2 was used, i.e., $0 \le \alpha \le 0.2$. Thus, equation (2) including an additional hysteretic delay t_{add} was rewritten as:

$$\beta(t) = e^{-\kappa_1 (t + t_{add})} \tag{3}$$

with

$$t_{add} = -\kappa_1^{-1} \ln(1-\alpha)$$

Equations (2) and (3) only deal with the bulk erosion. However, surface erosion also occurs in the exposed scaffold elements to the ISF. For the surface erosion, the larger contact area between a scaffold element and the ISF is, the faster the element degrades. Therefore, we introduced κ_2 to include the surface erosion, and $f(t)$ represents the number of ISF elements around a scaffold element in a 3×3×3 zone at time t in the degradation. Based on equation (3), the modified degradation rate was written as:

$$\frac{\mathrm{d}\beta(t)}{\mathrm{d}t} = -\left[1+\ln\left(1+\left(\frac{f(t)}{\kappa_2}\right)^2\right)\right]\kappa_1 e^{-\kappa_1(t+t_{add})} \tag{4}$$

It is worth mentioning that the polymer degradation is commonly known to be accelerated by the local carboxylic acid products, and the products play an important role in the autocatalytic effect. The effect has been verified in the experiments of the local hydrolysis [29, 30] and included in a theoretical model [10], however, we here would not take the auto-catalytic effect into consideration. Then, the judgment 1 arrives as:

Judgment 1: The scaffold (χ = 1) is completely degraded when $\beta(t)$ calculated from equation (4) is less than a threshold β_{thre}, i.e. $\beta(t)<\beta_{thre}$, and it is changed into the ISF, i.e., χ from 1 to 3.

Stochastic degradation: Equation (4) corresponds to a first order Erlang stochastic process [8], and it was used to define the hydrolytic probability density function $p(t)$ of scaffold element:

$$p(t) = N\left[1+\ln\left(1+\left(\frac{f(t)}{\kappa_2}\right)^2\right)\right]\kappa_1 e^{-N\kappa_1(t+t_{add})} \tag{5}$$

with

$$N = \ln(n)/\ln(m)$$

where n is the element number per unit volume in the present work, m is the reference element number per unit volume in literature [10], which influences the degradation rate constant κ_1, and N represents the relationship between the present element number n and the reference element number m. According to Gopferich's theory [9], the degradation probability (5) was related to the element number per unit volume, namely, the complete degradation of a scaffold with a smaller element number in a unit volume needs a longer time than that with a larger element number. Then, the second judgment reads as:

Judgment 2: The scaffold element completely degrades when a randomly generated number between 0 and 1 is less than p(t), and it is changed into the ISF, i.e., χ from 1 to 3.

The scaffold completely degrades when either of the judgments is satisfied. Typically, the mechanical properties of polymers were exponentially related to its molecular weight; for the present model, the Young's modulus $E_s(t)$ of the scaffold element was also exponentially related to $\beta(t)$. Although the experimental result does not show strictly exponential variation, the exponential decrease of Young's modulus is similar to the numerical result [29] and experimental result [30], i.e.:

$$E_s(t) = \left(E_s - E_{ISF}\right) \cdot \frac{e}{e-1}\left(1 - e^{-\beta(t)}\right) + E_{ISF} \tag{6}$$

where E_s and E_{ISF} are the ideal Young's moduli of the non-degraded scaffold and ISF, respectively. As stated before, for ideal scaffold element without initial degradation (i.e., t=0, t_{add}=0), we have $\beta(0)$=1, $E_s(0)$=E_s. When the scaffold is completely degraded at time t, we have $\beta(t)$=0, and the scaffold element is changed into the ISF, $E_s(t)$=E_{ISF}.

2.3. Bone remodeling

Bone remodeling under mechanical stimulus is complex, but generally, it consists of bone resorption and formation. It is reported that only the osteoclasts and osteoblasts adhering on the surface of the scaffold or bone can sense the mechanical signal [31], and further resorb and form bone tissue. Therefore, the bone resorption and formation is considered to only occur on the surface of the scaffold or newly-formed bone. In addition, osteoblasts on the surfaces of the extravascular bone matrix [32] and osteocytes residing in the lacunae [33] were directly stimulated by the fluid shear stress, or hydrostatic pressure. However, the structural strain or strain-related instead of the shear stress or hydrostatic pressure were widely used to regulate the bone remodeling process, actually the strain or strain-related stimulus indirectly influences the cell activities because it causes the changes of the ISF flow and the hydrostatic pressure. Moreover, there is an indication that immature bone is more responsive to alterations of cyclic strains than mature bone [34]. Thus, the local nonuniform strain energy density (SED) ψ was here used as the mechanical stimulus. Based on the Husikes theory [15] and Schulte's work [35], the bone remodeling rate $u(\psi)$, indicating the thickness variation of formed/resorbed bone in a unit time, is depicted in Figure 3, and mathematically expressed as:

$$u(\psi)=\begin{cases} -u_{\max} & \psi<\psi_{\text{lower}}-u_{\max}/c \\ -c(\psi_{\text{lower}}-\psi) & \psi_{\text{lower}}-u_{\max}/c<\psi<\psi_{\text{lower}} \\ 0 & \psi_{\text{lower}}<\psi<\psi_{\text{upper}} \\ c(\psi-\psi_{\text{upper}}) & \psi_{\text{upper}}<\psi<\psi_{\text{upper}}+u_{\max}/c \\ u_{\max} & \psi_{\text{upper}}+u_{\max}/c<\psi \end{cases} \tag{7}$$

where c is a constant denoting how fast bone formation and resorption rates reach the maximum growth rate $u_{\max}$, ψ_{upper} and ψ_{lower} are bone formation and resorption thresholds, respectively. Between the two thresholds is the 'lazy zone', which represents equilibrium between the resorption rate and the formation rate. The local SED ψ of element i is influenced by its neighboring element j within a sensitive distance D, and the closer the jth element to the ith element is, the greater it contributes, and the local SED is expressed as [35]:

$$\psi(x_i)=\sum_{j=1}^{q} e^{-\frac{\mathrm{d}(x_j-x_i)^2}{2D^2}}\,\mathrm{SED}(x_j) \tag{8}$$

where q is the number of the contributive elements. $\mathrm{SED}(x_j)$ is the strain energy density of the

jth element, and d(x_j-x_i) is the distance between element i and j. According to the remodeling rate $u(\psi)$, the bone volume fraction $\alpha_b(t)$ of a bone element in the dynamic process increases or decreases, and its rate is defined as:

$$\frac{\mathrm{d}\alpha_b(t)}{\mathrm{d}t} = \frac{u(\psi)}{l} \tag{9}$$

Here, unmatured bone elements are cellular and share a constituent material (matured bone), then, the bone volume fraction $\alpha_b(t)$ equals the ratio of the density $\rho_b(t)$ of the unmatured bone to the density ρ_b of the matured bone, i.e., $\alpha_b(t) = \bar{\rho}_b(t) = \rho_b(t)/\rho_b$. The relative density $\bar{\rho}_b(t)$ is a primary parameter to determine the Young's modulus $E_b(t)$ of the cellular bone. According to the Gibson's work [25], the density-modulus relationship $E_b(t) = A\bar{\rho}_b(t)^B$ is often employed to describe the Young's modulus of porous bones [36]. Meanwhile, considering two extreme cases, $E_b(0)=E_{ISF}$ (i.e., $\bar{\rho}_b(0)=0$) and $E_b(t)=E_b$ (i.e., $\bar{\rho}_b(t)=1$), a modified density-modulus relationship is developed as:

$$E_b(t) = (E_b - E_{ISF})\bar{\rho}_b(t)^3 + E_{ISF} = (E_b - E_{ISF})\alpha_b(t)^3 + E_{ISF} \tag{10}$$

It is worth mentioning that the empirical equations (6) and (10) satisfy the extreme cases, but rigorous solutions can be obtained by employing complex micromechanical models for the mechanical properties of the scaffold degradation [37] and bone formation [38, 39].

Like the scaffold degradation judged by molecular weight, the relative density $\bar{\rho}_b(t)$ or bone volume fraction $\alpha_b(t)$ is used to judge the bone remodeling, since it denotes the degree of bone maturation and determines the mechanical properties of bone. Plus, when $\alpha_b(t)$ is small, an element does not contribute to mechanical properties of the scaffold-bone system. Then, the judgment goes as follows:

When the bone volume fraction $\alpha_b(t)$ of an element is less than a threshold α_{thre}, the element is changed into ISF, i.e., χ from 2 to 3. On contrary, when $\alpha_b(t)$ of an element is greater than α_{thre}, the element is changed into bone, i.e., χ from 3 to 2.

3. RESULTS

3.1. Input parameters

The scaffold here is constituted by PLA. The element number per unit volume *m* in the literature [10] is 100^3, and the counterpart in this work is 2^3, thus, *N* in equation (5) was calculated as $N=\ln(2^3)/\ln(100^3)=0.15$. For the bone remodeling, the maximum resorption or formation rate is 2 $mm^3/mm^2/yr$ [40], which corresponds to u_{max}=0.005 mm/day in the present simulations. The thresholds ψ_{lower} and ψ_{upper} were modified from literature [35]. Besides, as stated in Section 2.1, the rehabilitation exercise level was 3 MPa. All inputting parameters used in the simulation are listed in Table 1.

Table 1 Input parameters of the simulations.

Parameters		Value	Unit
Bulk degradation rate constant	κ_1	0.0185[10]	day^{-1}
Surface degradation rate constant	κ_2	6	-
Ratio	N	0.15	-
Constant	c	0.5[35]	$mm \cdot MPa^{-1} \cdot day^{-1}$
Maximal formation/resorption velocity	u_{max}	0.005[40]	$mm \cdot day^{-1}$
Resorption threshold	ψ_{lower}	0.01[35]	MPa
Formation threshold	ψ_{upper}	0.02[35]	MPa
Influence distance	D	52[35]	μm
Young's modulus of mature bone	E_b	20[41]	GPa
Ideal Young's modulus of undegraded PLA	E_s	5[42]	GPa
Poisson's ratio of scaffold and bone	υ	0.3	-

Young's modulus of ISF	E_{ISF}	0.01	GPa
Poisson's ratio of ISF	Y_{ISF}	0.49	-
State change threshold	α_{thre}	0.01	-
	β_{thre}	0.01	

3.2. Simulation results

In this part, the seven exercise durations and the non-exercise case were simulated.

3.2.1. The scaffold degradation and bone formation.

The volumes of the degraded scaffold and the formed bone normalized by the RVC volume are plotted in Figure 4. Generally, it shows that the conflict of the trends of the scaffold degradation and bone formation, and the scaffold completely degrades and bone formation reaches a stable state after 140 days. In their respective process, different exercise cases share a similar trend. For the scaffold, the degradation described by equations (4) and (5) is not influenced by the mechanical stimulus, thus, the degradation for all cases is close to the non-exercise case (OSD in Figure 4a). Whereas, the degradation difference for all cases after 20 days exists, and this is induced by the coupling of the bone formation, which is remodeled by the stimulus. For the newly-formed bone, bone rarely forms in initial 20 days and reaches a temporary balance before 50 days; afterwards, bone keeps forming until 140 days (Figure 4b). Moreover, the bone forms faster in a larger exercise durations than that in smaller durations before 50th day, while the final bone formation in all cases is similar except for the case of 0.2.

3.2.2. The case of rehabilitation exercise duration 0.5.

To observe the coupling process, we exemplified the case of 0.5, and states at nine time points were snapshot in Figure 5. For the sake of the clarity, Figure 5 only displays the maturation degree of formed bone by gray values, and the degradation degree of scaffold is shown in the Appendix. Before day 10, scaffold changes weakly (Figure 5a), and there is almost no newly formed bone tissue (the black line in Figure 5b), but the system's Young's modulus in the loading direction decreases quickly and monotonously (the blue line in Figure 5b). This is because only a portion of PLA molecular chains in the scaffold element breaks (equation (4)), which results in a decrease in the molecular weight and a further decrease in Young's modulus of the element. However, this does not mean that the element is completely degraded, thus the volume of the scaffold element is not reduced significantly (the red line in Figure 5b). From day 10 to day 60, scaffold degrades much faster than before, and more scaffold elements are degraded (Figure 5a). This is because more and more voids forming in the degraded scaffold facilitate the degradation as the process proceeds. The bone firstly forms on the surface of the four pillars along the loading direction, especially at the eight corners of the RVC because of the high mechanical stimulus. Meanwhile, the Young's modulus of the coupling structure stays constantly around 480 MPa and forms a plateau (Figure 5b), which roughly corresponds to the temporary balance in Figure 4b. From day 60 to day 150, the scaffold keeps degrading and almost fully disappears at day 120 (Figure 5a), and the fast scaffold degradation promotes the bone formation till day 120. Moreover, the Young's modulus increases greatly because of the formed bone. After 150 days, the scaffold completely degrades, and the bone remodeling reaches a balance except few unmatured bone elements, which represents the successful bone tissue regeneration.

3.2.3. The comparison of Young's modulus between all cases.

For all the exercise cases, their Young's moduli of the scaffold-bone system are reported in Figure 6, and they share a similar variation. According to the specific case in Section 3.2.2, we divide the process into four stages. At stage I (0-15 days), there is almost no difference in the Young's moduli between all cases. This is because there is not much polymer scaffold degradation and new bone formation, and the scaffold degradation is unrelated to the mechanical stimulus. At stage II (15-80 days), bone starts to form. Different from the degraded scaffold, bone formation is influenced by the stimulus, which results in the disparity between different cases as the process proceeds. At the beginning of this stage, the modulus of the system continues decreasing till 50th day, after that it increases slightly due to newly-formed bone, and the modulus reaches a minimum of the entire process. At stage III (80-140 days), the Young's modulus increases dramatically due to the degraded scaffold, which leads to a fast bone formation. At stage IV (after 140 days), the Young's modulus becomes stable due to the completely formed bone. It is worth mentioning that at stages II, the longer the exercise duration per day is, the greater the modulus attains, as shown in Figure 4b; whereas, at stage III, the system's modulus reverses at 100th day, i.e., the less exercise duration produces a greater modulus. Regarding the reversal at stage III, it may be caused by the fast bone formation with greater exercise durations at stage II, which results in a bone coat around the scaffold, and the coat mitigates the scaffold degradation. Thus, the formed bone under a greater duration is less than that under a smaller duration at stage III, but the scaffold-bone system in a greater duration matures early than those in a smaller duration. Interestingly, at stage IV, the case of 0.3 has an optimal final modulus, and this indicates that the excessive physical exercise may be not beneficial for the bone regeneration.

4. Discussions

The dynamic bone repair process under different exercise durations were investigated and modeled by coupling the scaffold degradation and bone remodeling. Basic materials were assumed to be isotropic and linear-elastic, but the real bone tissue is anisotropic also due to the hierarchical arrangement (from nano- to macro-scale) of its components, and the multilevel structure plays a critical role in determining the mechanical properties of the bone [43, 44]. Materials' anisotropy influences the inter-level or intra-level cracking behavior in the biomaterials-bone system [44], and the elastic constants or the strain distribution in an organ after implantation [45]. However, here, due to the only existence of the polymer in the scaffold, the polymer was considered as an isotropic linear elastic material. The scaffold structure's anisotropy can be achieved by differentiating the side sizes of the scaffold in its three orthotropic directions, and this could be used to tailor a suitable scaffold to match the anisotropic natural bone.

The scaffold degradation is caused by hydrolysis. By adding an extra term $f(t)/\kappa_2$, the surface erosion was incorporated into the model due to surface contact with ISF, which accelerated the degradation. We compared the number average molecular weight (M_n) in the present simulation with its counterparts in experiments in literature in Figure 7. Generally, the present degradation exhibits an exponential decay, and is comparable to the literatures [46-50]. In particular, at the early stage of degradation, from 0 to 20 days, the number average molecular weight (M_n) of the scaffold linearly decreased by 40%, while the volume percentage of scaffold in the RVC (SV/TV) only decreased by 10% (Figure 4a). This is similar to the literature [46, 47], which reported that the PLA scaffold weight slowly reduced before 20 days (5% and 15% respectively), but M_n was lost almost 50% in *in vitro* experiments. After 20 days, both M_n and SV/TV decreased until a compete degradation at around 150th day. Scaffold's size as well as shape also influence the polymer degradation, thus they are always optimized from the sense of the physical (mechanics, permeability) and biochemical properties (cell migration, tissue formation). When the size of the PLA matrix is smaller than a critical size, the surface erosion prevails in the degradation process.

This is because a larger specific surface area allows a greater contact with water-contained ISF, which facilitates the hydrolytic reaction of the matrix. The scaffold shape seems to have a weak influence on the bone-repair dynamic process [51]. However, Adachi et al [21] and Chen et al. [22] studied two kinds of scaffold RVC with different shapes, And reported that the neo-tissue firstly forms at the corner in the former work and on the inner surface in the latter work. this is beneficial for the design of scaffold architectures, for instance, on basis of the optimized size and shape, the distribution of the polymer mass can be tailored to balance the scaffold degradation and new bone formation [21,22,52]. Besides, temperature and pH of the hydrolytic environment have an effect on the degradation rate, and molecular weight also determines the degradation time [53]. Thus, the totally PLA degradation time differs from six months to two years [54], and the degradation parameters in the present simulation could be modified to address different situations.

The bone remodeling is on basis of a SED-regulated mechanosensory function. At the final stage, the volume percentage of formed bone in the RVC (BV/TV) of all exercise cases, except 0.2, is 15 % ± 1 %, corresponding to an approximate constant porosity of 85% (Figure 4b). The constant porosity is determined by the geometry (or pillar thickness) of the RVC, and this verifies that the final trabeculae thickness is closely associated with the magnitude of the mechanical stimulus [55], and here the applied load is kept to be 3 MPa. The peak strain of the final scaffold-bone system is 1625 ± 254 με (Figure 8). According to the "mechanostat" model proposed by Frost [56], the bone remodeling reaches homeostasis, and the remodeled bone mass and strength keep constants when the peak strain is between 1000 με and 1500 με (Modeling Region, MESm), which is close to the present mean value 1625με.

For the coupling model, from Figure 5a, we can see that there is no formed bone tissue along the horizontal pillars. This is due to the weak mechanical stimulus at the pillars, which is not able to promote bone formation. This phenomenon is consistent with the numerical simulation by van Oers et al. [57], in which it has been shown that the strain-induced osteocyte signal only directed the bone remodeling in the loading direction. Moreover, this also explains that trabecula in cancellous bone always orientates along the loading direction. From Figure 6, it is seen that under the same exercise pressure 3 MPa, the system reaches a minimum state around 50 days and a balance state around 140 day regardless of the exercise durations. This is also comparable to the work by Adachi et al. [21], who reported that the optimal scaffold with was completely degraded after 120 days, and the system's strain energy was the weakest at day 40. However, it is worth mentioning that they used the strain energy instead of the Young's modulus as the optimal index of the scaffold. In order to monitor the system's Young's modulus in the entire process, the smallest Young's modulus and the final Young's modulus are plotted in Figure 9, and they are 280 ± 150 MPa and 1900 ± 300 MPa, respectively.

Clinically, the presented coupled results suggest that rehabilitation exercise is unnecessary in the first two weeks as it has slight effect on bone remodeling process. After this period, because a longer exercise time produces a smaller final modulus of the scaffold-bone system, moderating exercise time per day is recommended to obtain a final optimal structural modulus. Here, 0.3 is the best choice for the optimal bone repair.

Indeed, due to simplifications of the scaffold degradation and bone remodeling, there are several limitations. First, in reality, the polymer degradation is also influenced by the mechanical stimulus [58,59], composition, molecular weight, shape [60] and pH value [61] etc., but the present degradation model did not consider these factors. Meanwhile, the polymer degradation here only influences the stress redistribution of the scaffold-bone system, and the effect of the degradation on biological and molecular responses was not taken into account either. Second, the real walking frequency was generally treated as the mean loading history every day. Thirdly, the mechanical stimulus (SED) was considered as the only factor controlling the bone remodeling. The growth rate *c* as an empirical constant in equation (7) was selected, whereas actually, the growth rate is related to the biochemical and molecular signals etc., which regulate the activities of osteoclasts and osteoblasts [32,62]. Fourth, ISF was considered as incompressible solid instead of fluid, and this neglects the important role of the fluid shear stress (FSS) between ISF and bone tissue [63]. Despite these limitations, the novel framework still provides insight into the interplay between degraded scaffold and formed bone under different rehabilitation exercise durations, and helps to establish a sustainable link between the modelling and simulation and the tissue engineering communities.

5. CONCLUSIONS

This work investigated the influence of rehabilitation exercise durations on the bone repair by coupling the scaffold degradation and bone remodeling, which exhibit an opposite variation. The degraded scaffold dominates the stiffness of the scaffold-bone system at the initial stage, and the newly-formed bone dominates at the final stage. Under a cycled mechanical stimulus, a longer exercise duration leads to an earlier maturation of bone but a lower final Young's modulus. The final Young's modulus is approximate 1.9 GPa, which is comparable to that of the trabecular bone. Although the theory is based on the simplified mathematical model, it still improves our understanding of the dynamic bone remodeling process, and suggests that moderate exercise duration is beneficial for the bone repair. Furthermore, it can be used to guide the design of polymer scaffolds for future clinical applications.

Appendix:

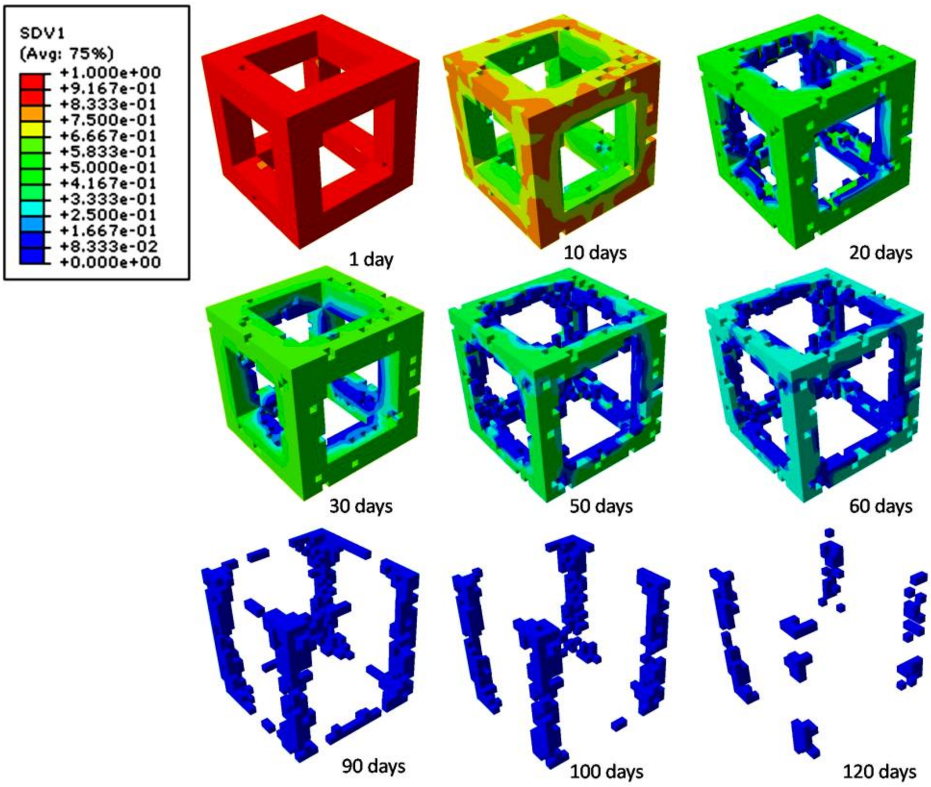

Figure A. Snapshots of the evolving process of the degraded scaffold at different time points

ACKNOWLEDGEMENTS

This study was supported by the Natural Science Foundation of China (NSFC) (No. 31300780, 11272091, 11422222, 31470043, 11772093), the Fundamental Research Funds for the Central Universities (No. 2242016R30014), and partially supported by the National 973 Basic Research Program of China (No. 2013CB733800) and ARC (FT140101152). N.M.P. is supported by the European Commission H2020 under the Graphene Flagship Core 1 No. 696656 (WP14 "Polymer Composites"), and FET Proactive "Neurofibre" Grant No. 732344.

Conflict of interest

The authors declare that they have no conflict of interests.

REFERENCES

[1]. Lewandrowski KU, Gresser JD, Wise DL, et al. Bioresorbable bone graft substitutes of different osteoconductivities: a histologic evaluation of osteointegration of poly (propylene glycol-co-fumaric acid)-based cement implants in rats. Biomaterials 2000;21(8):757-64.

[2]. Cao H, Kuboyama N. A biodegradable porous composite scaffold of PGA/β-TCP for bone tissue engineering. Bone, 2010;46(2):386-95.

[3]. Chen Q, Baino F, Spriano S, et al. Modelling of the strength–porosity relationship in glass-ceramic foam scaffolds for bone repair. J Eur Ceram Soc 2014;34(11):2663-73.

[4]. Huang S, Chen Z, Pugno N, et al. A novel model for porous scaffold to match the mechanical anisotropy and the hierarchical structure of bone. Mater Lett 2014;122:315-9.

[5]. Courteix D, Lespessailles E, Peres SL, et al. Effect of physical training on bone mineral density in prepubertal girls: A comparative study between impact-loading and non-impact-loading sports. Osteoporos Int 1998;8(2):152-8.

[6]. Gopferich A. Mechanisms of polymer degradation and erosion. Biomaterials 1996;17(2):103-14.

[7]. Langer R, Peppas N. Chemical and physical structure of polymers as carriers for controlled release of bioactive agents: A review. J Mater Sci Part C1983;23(1):61-126.

[8]. Gopferich A, Langer R. Modeling of polymer erosion. Macromolecules 1993;26:4105-12.

[9]. Gopferich A. Polymer Bulk Erosion. Macromolecules 1997;30:2598-604.

[10]. Chen Y, Zhou S, Li Q. Mathematical modeling of degradation for bulk-erosive polymers: Applications in tissue engineering scaffolds and drug delivery systems. Acta Biomater 2011;7(3):1140-9.

[11]. Siepmann J, Gopferich A. Mathematical modeling of bioerodible, polymeric drug delivery systems. Adv Drug Deliv Rev 2001;48(2-3):229-47.

[12]. von Burkersroda F, Schedl L, Gopferich A. Why degradable polymers undergo surface erosion or bulk

erosion. Biomaterials 2002;23:4221-31.

[13]. Carter DR, Orr TE, Fyhrie DP. Relationships between loading history and femoral cancellous bone architecture. J Biomech 1989;22:231-44.

[14]. Frost HM. The laws of bone structure. C.C. Thomas. 1964.

[15]. Huiskes R, Weinans H, Grootenboer HJ, Dalstra M, Fudala B, Slooff TJ. Adaptive bone-remodeling theory applied to prosthetic-design analysis. J Biomech 1987;20:1135-50.

[16]. Sturm S, Zhou S, Mai YW, Li Q. On stiffness of scaffolds for bone tissue engineering-a numerical study. J Biomech 2010; 43(9):1738-44.

[17]. Cowin SC, Hegedus DH. Bone remodeling I: Theory of adaptive elasticity. J Elasticity1976;6:313-26.

[18]. Carter DR. Mechanical loading histories and cortical bone remodeling. Calcif Tissue lnt 1984;36:S19-24.

[19]. Fyhrie DP, Carter DR. A unifying principle relating stress to trabecular bone morphology. J Orthop Res 1986;4:304-17.

[20]. Adachi T, Tsubota K, Tomita Y. Trabecular surface remodeling simulation for cancellous bone using microstructural voxel finite element models. J Biomech Eng 2001;123(5):403-9.

[21]. Adachi T, Osako Y, Tanaka M, Hojo M, Hollister SJ. Framework for optimal design of porous scaffold microstructure by computational simulation of bone regeneration. Biomaterials 2006;27(21):3964-72.

[22]. Chen Y, Zhou S, Li Q. Microstructure design of biodegradable scaffold and its effect on tissue regeneration. Biomaterials 2011;32:5003-14.

[23]. Carter DR, Spengler DM. Mechanical properties and composition of cortical bone. Clin Orthop Relat R 1978;135:192-217.

[24]. Hillsley MV, Frangos JA. Bone tissue engineering: the role of interstitial fluid flow. Biotechnol Bioengin 1994;43(7):573-81.

[25]. Gibson LJ. The mechanical behaviour of cancellous bone. J Biomech 1985;18(5):317-28.

[26]. Shefelbine SJ, Augat P, Claes L, Simon U. Trabecular bone fracture healing simulation with finite element analysis and fuzzy logic. J Biomech 2005;38(12):2440-50.

[27]. Zhang M, Yang Z, Chow LL, et al. Simulation of drug release from biodegradable polymeric microspheres with bulk and surface erosions. J Pharm Sci 2003;92(10):2040-56

[28]. Ferrero C, Bravo I, Jiménez-Castellanos MR. Drug release kinetics and fronts movement studies from methyl methacrylate (MMA) copolymer matrix tablets: effect of copolymer type and matrix porosity. J Control Release 2003;92(1):69-82.

[29]. Wang Y, Han X, Pan J, et al. An entropy spring model for the Young’s modulus change of biodegradable polymers during biodegradation. J Mech Behav Biomed Mater 2010;3(1):14-21.

[30]. Tsuji H. Autocatalytic hydrolysis of amorphous-made polylactides: Effects of L-lactide content, tacticity, and enantiomeric polymer blending. Polymer 2002;43(6):1789-96.

[31]. Horwithz AR, Parsons JT. Cell migration-movin' on. Science 1999;286(5542):1102-3.

[32]. Scheiner S, Pivonka P, Hellmich C. Coupling systems biology with multiscale mechanics, for computer simulations of bone remodeling. Comput Method Appl Mech Eng 2013;254:181-96.

[33]. Scheiner S, Pivonka P, Hellmich C. Poromicromechanics reveals that physiological bone strains induce osteocyte-stimulating lacunar pressure. Biomech Model Mechanobiol 2016;15(1):9-28.

[34]. Hou JC, Salem GJ, Zernicke RF, et al. Structural and mechanical adaptations of immature trabecular bone to strenuous exercise. J Appl Physiol 1990;69(4):1309-14.

[35]. Schulte FA, Zwahlen A, Lambers FM, Kuhn G, Ruffoni D, Betts D, Webster DJ, Muller R. Strain-adaptive in silico modeling of bone adaptation–A computer simulation validated by in vivo micro-computed tomography data. Bone 2013;52(1):485-92.

[36]. Keller TS. Predicting the compressive mechanical behavior of bone. J Biomech 1994;27(9):1159–68.

[37]. Luczynski K W, Dejaco A, Lahayne O, et al. MicroCT/micromechanics-based finite element models and

quasi-static unloading tests deliver consistent values for Young's modulus of rapid-prototyped polymer-ceramic tissue engineering scaffold. Comput Model Eng Sci 2012;87(6):505-28.

[38]. Hellmich C, Ulm FJ, Dormieux L. Can the diverse elastic properties of trabecular and cortical bone be attributed to only a few tissue-independent phase properties and their interactions?. Biomech Model Mechanobiol 2004;2(4):219-38.

[39]. Blanchard R, Dejaco A, Bongaers E, et al. Intravoxel bone micromechanics for microCT-based finite element simulations. J Biomech 2013;46(15):2710-21.

[40]. Frost HM. Skeletal structural adaptations to mechanical usage (SATMU): 2. Redefining Wolff's law: the remodeling problem. Anat Rec 1990;226(4):414-22.

[41]. Morgan TG, Bostrom MP, van der Meulen MC. Tissue-level remodeling simulations of cancellous bone capture effects of in vivo loading in a rabbit model. J Biomech 2015;48(5):875-82.

[42]. Middleton JC, Tipton AJ. Synthetic biodegradable polymers as orthopedic devices. Biomaterials 2000;21(23):2335-46.

[43]. Fritsch A, Hellmich C. 'Universal' microstructural patterns in cortical and trabecular, extracellular and extravascular bone materials: Micromechanics-based prediction of anisotropic elasticity. J Theor Biol 2007; 244(4):597-620.

[44]. Scheiner S, Komlev VS, Hellmich C. Strength increase during ceramic biomaterial-induced bone regeneration: a micromechanical study. Int J Fract 2016;202(2):217-35.

[45]. Hellmich C, Kober C, Erdmann B. Micromechanics-based conversion of CT data into anisotropic elasticity tensors, applied to FE simulations of a mandible. Ann Biomed Eng 2008;36(1):108.

[46]. Tsuji H, Eto T, Sakamoto Y. Synthesis and hydrolytic degradation of substituted poly(DL-Lactic Acid)s. Materials 2011;4(8):1384-98.

[47]. Helder J, Dijkstra PJ, Feijen J. In vitro degradation of glycine/DL-lactic acid copolymers. J Biomed Mater

Res1990; 24(8):1005-20.

[48]. Chawla AS, Chang TM. In-vivo degradation of poly(lactic acid) of different molecular weights. Biomater Med Devices Artif Organs 1985-1986;13(3-4):153-62.

[49]. Pitt CG, Gratzl MM, Kimmel GL, Surles J, Schindler A. Aliphatic polyesters II. The degradation of poly (DL-lactide), poly (epsilon-caprolactone), and their copolymers in vivo. Biomaterials 1981;2(4):215-20.

[50]. Pistner H, Bendix DR, Muhling J, Reuther JF. Poly(L-lactide): a long-term degradation study in vivo. Part III. Analytical characterization. Biomaterials 1993;14(4):291-8.

[51]. McIntosh L, Cordell JM, Johnson AJW. Impact of bone geometry on effective properties of bone scaffolds. Acta Biomater 2009;5(2):680-92.

[52]. Hollister SJ, Maddox RD, Taboas JM. Optimal design and fabrication of scaffolds to mimic tissue properties and satisfy biological constraints. Biomaterials 2002;23(20):4095-103.

[53]. Wu XS, Wang N. Synthesis, characterization, biodegradation, and drug delivery application of biodegradable lactic/glycolic acid polymers. Part II: biodegradation. J Biomater Sci Polym Ed 2001;12(1):21-34.

[54]. Sinclair RG. The case for polylactic acid as a commodity packaging plastic. J Macromole Sci Part A 1996;A33(5):585-97.

[55]. Ruimerman R, Hilbers P, van Rietbergen B et al. A theoretical framework for strain-related trabecular bone maintenance and adaptation. J Biomech 2005;38(4):931-41.

[56]. Frost HM. Bone’s mechanostat: a 2003 update. Anat Rec 2003;275:1081–101.

[57]. van Oers RFM, Ruimerman R, Tanck E, et al. A unified theory for osteonal and hemi-osteonal remodeling. Bone 2008;42(2):250-9.

[58].Thompson DE, Agrawal CM, Athanasiou K. The effects of dynamic compressive loading on biodegradable implants of 50-50% polylactic Acid-polyglycolic Acid. Tissue Eng 1996;2(1):61-74.

[59]. Fan YB, Li P, Zeng L, Huang XJ. Effects of mechanical load on the degradation of poly(D,L-lactic acid) foam.

Polym Degrad Stab 2008;93(3):677-83.

[60]. Cao Y, Mitchell G, Messina A, et al. The influence of architecture on degradation and tissue ingrowth into three-dimensional poly (lactic-co-glycolic acid) scaffolds in vitro and in vivo. Biomaterials 2006;27(14):2854-64.

[61].Li H, Chang J. pH-compensation effect of bioactive inorganic fillers on the degradation of PLGA. Compos Sci Technol 2005;65(14):2226-32.

[62]. Scheiner S, Pivonka P, Smith DW, et al. Mathematical modeling of postmenopausal osteoporosis and its treatment by the anti-catabolic drug denosumab. Int J Numer Method Biomed Eng 2014;30(1):1-27.

[63]. Dillaman RM, Roer RD, Gay DM. Fluid movement in bone: theoretical and empirical. J Biomech 1991;24 suppl 1:163-77.

Figure Captions:

Figure 1. Periodic scaffold. (a) Scaffold architecture; (b) Representative volume cell (RVC).

Figure 2. Exercise duration per day and mesh of the RVC. (a) Exercise duration exercise described by trapezoidal loading pulse in a day; (b) Initial computation domain including 8000 elements, in which the scaffold and ISF elements are red and white, respectively.

Figure 3. Bone remodeling velocity $u(\psi)$ *vs*. strain energy density ψ.

Figure 4. The change of SV/TV (a) and BV/TV(b) with time after scaffold implantation for seven exercise durations and non-exercise case (only scaffold degradation, OSD). (BV: Bone Volume, SV: Scaffold Volume, TV: Total Volume)

Figure 5. The dynamic process of scaffold-bone system with exercise duration 0.5. (a) Snapshots of the scaffold-bone system at different time points, note that the blue elements are scaffold and others are bone. To observe the maturation degree of formed bone, the bone element is displayed from light grey to dark grey; (b) Variation of the Young's modulus, BV/TV and SV/TV.

Figure 6. Young's modulus of the scaffold-bone system under different exercise durations.

Figure 7. The comparison between our simulations and other measurements: In vitro degradation 1 (Tsuji et al. [46]), In vitro degradation 2 (Helder et al. [47]), in vivo degradation 1 (Pitt et al. [49]) and in vivo degradation 2 (Pistner et al. [50]).

Figure 8. The final strain of the seven exercise durations.

Figure 9. The final and lowest Young's modulus of the seven exercise durations during the bone-repair process.

Figure 1:

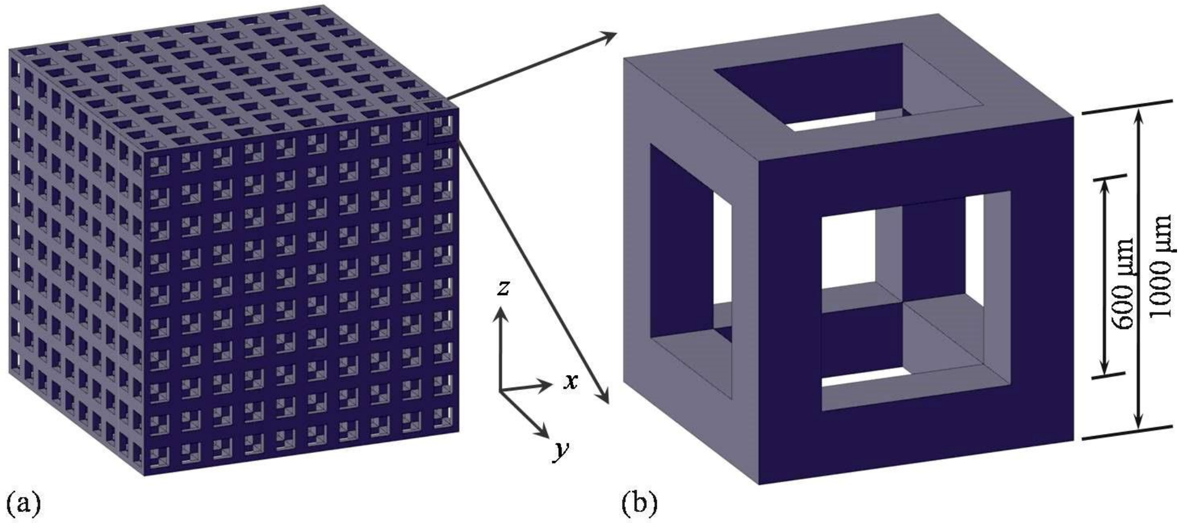

Figure 2:

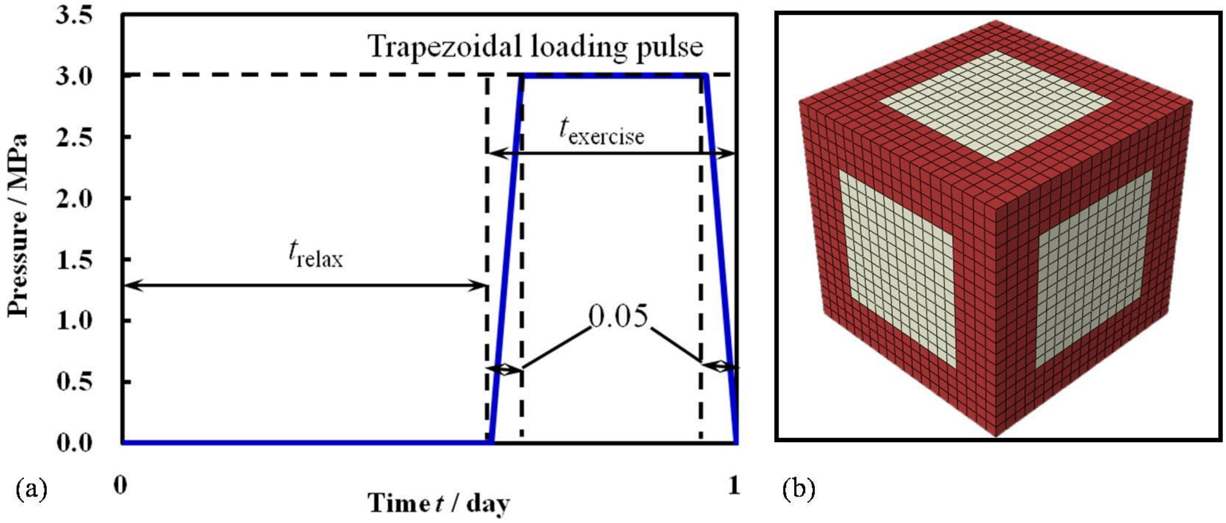

Trapezoidal loading pulse
Pressure / MPa
3.5
3.0
2.5
2.0
1.5
1.0
0.5
0.0
t_{exercise}
t_{relax}
0.05
0
1
Time t / day
(a)
(b)

Figure 3:

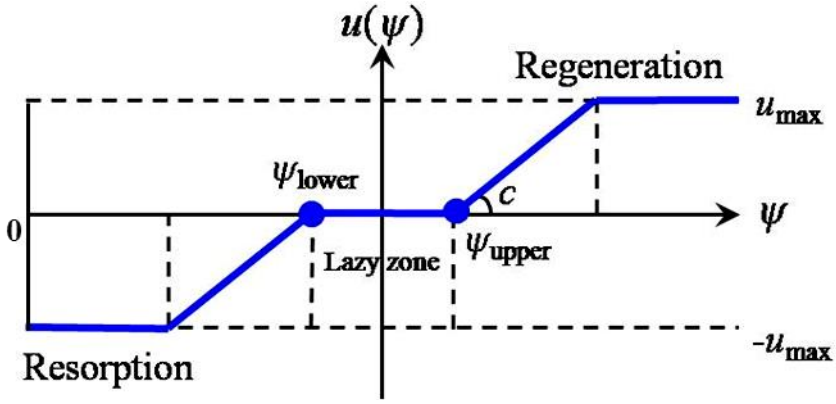

$u(\psi)$
Regeneration
u_{max}
ψ_{lower}
c
ψ
0
Lazy zone
ψ_{upper}
$-u_{max}$
Resorption

Figure 4:

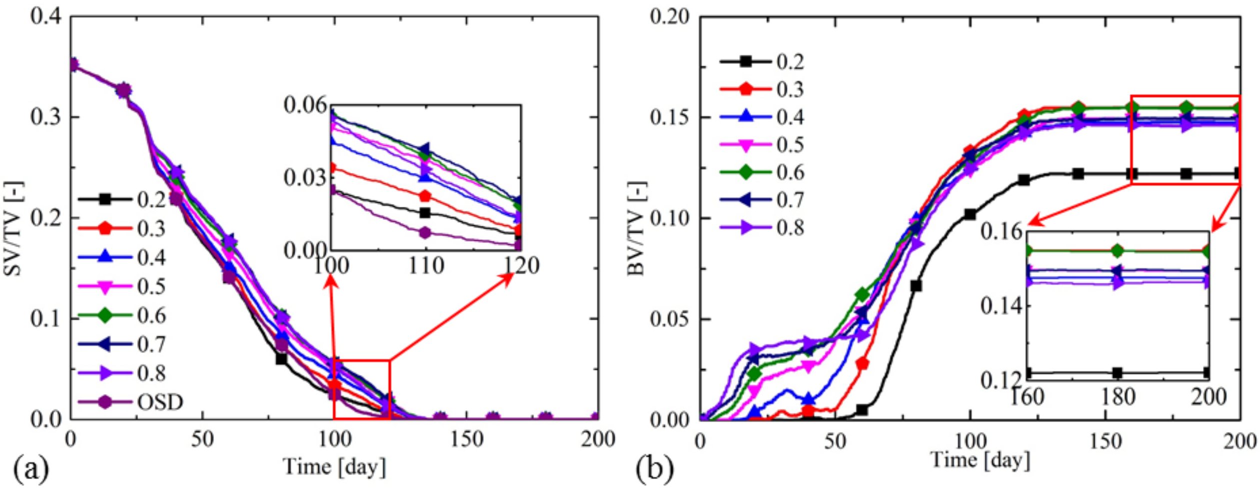

Figure 5:

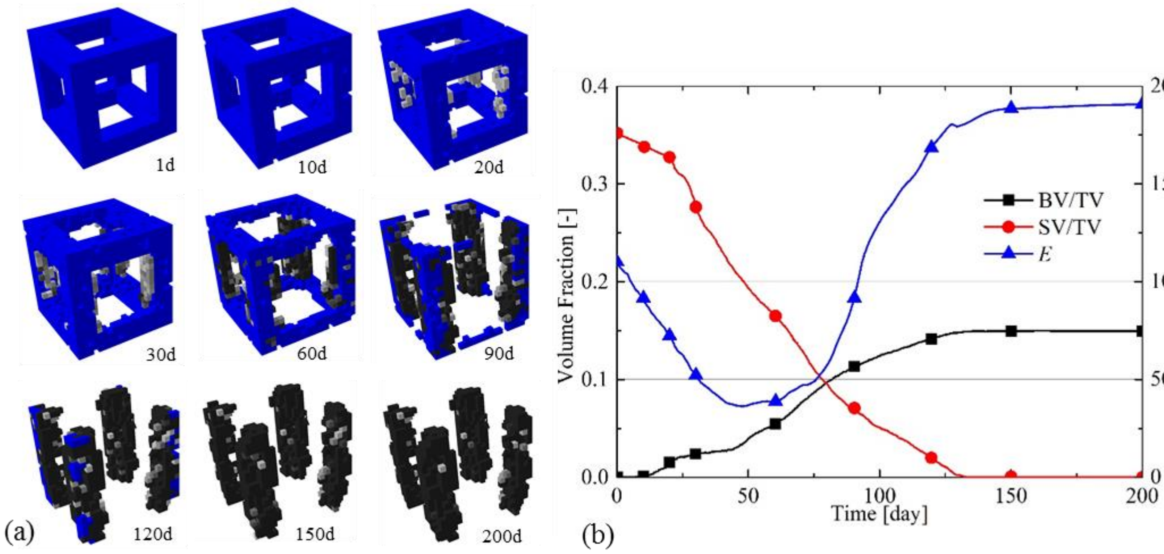
1d
10d
20d
30d
60d
90d
120d
150d
200d
(a)
Volume Fraction [-]
E [MPa]
Time [day]
BV/TV
SV/TV
E
0.0
0.1
0.2
0.3
0.4
0
500
1000
1500
2000
0
50
100
150
200
(b)

Figure 6:

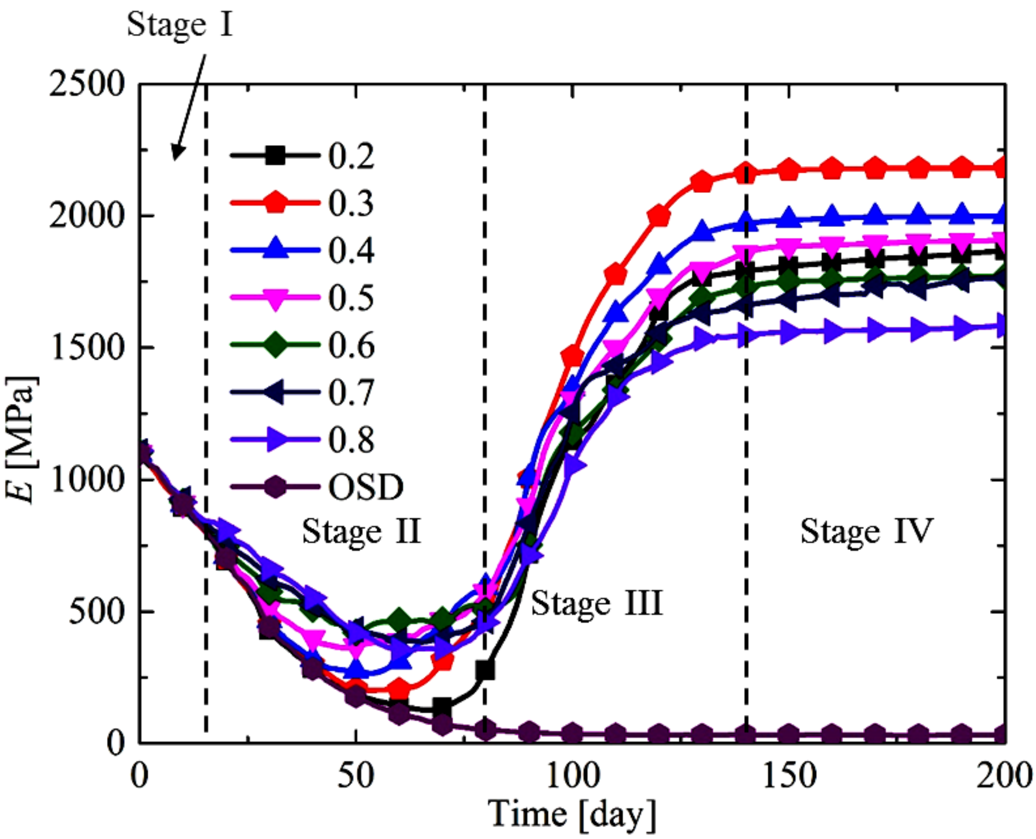

Stage I
Stage II
Stage III
Stage IV
0.2
0.3
0.4
0.5
0.6
0.7
0.8
OSD
E [MPa]
Time [day]
0
500
1000
1500
2000
2500
0
50
100
150
200

Figure 7:

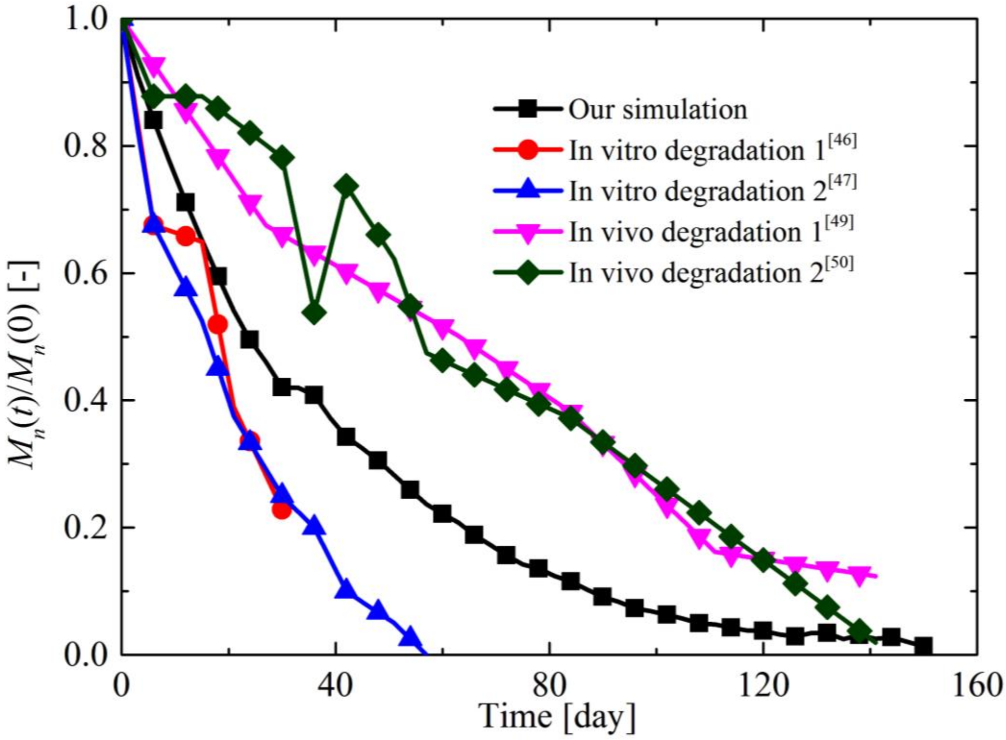

Our simulation
In vitro degradation 1[46]
In vitro degradation 2[47]
In vivo degradation 1[49]
In vivo degradation 2[50]
$M_n(t)/M_n(0)$ [-]
Time [day]
0.0
0.2
0.4
0.6
0.8
1.0
0
40
80
120
160

Figure 8:

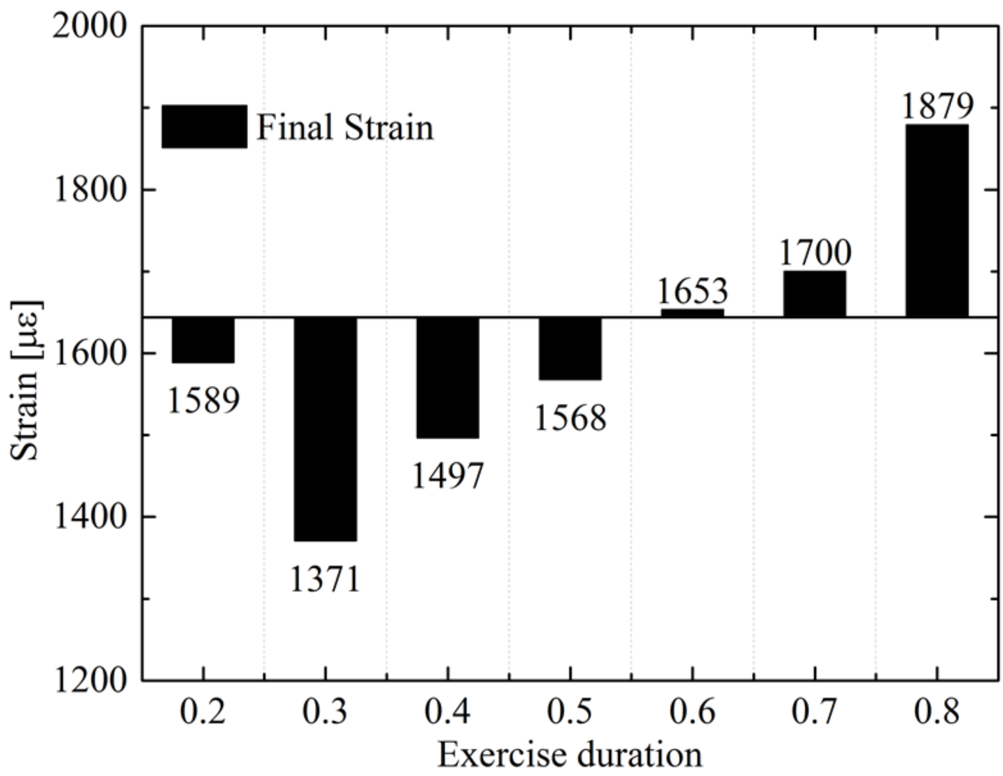

Final Strain
2000
1800
1600
1400
1200
Strain [με]
1589
1371
1497
1568
1653
1700
1879
0.2
0.3
0.4
0.5
0.6
0.7
0.8
Exercise duration

Figure 9:

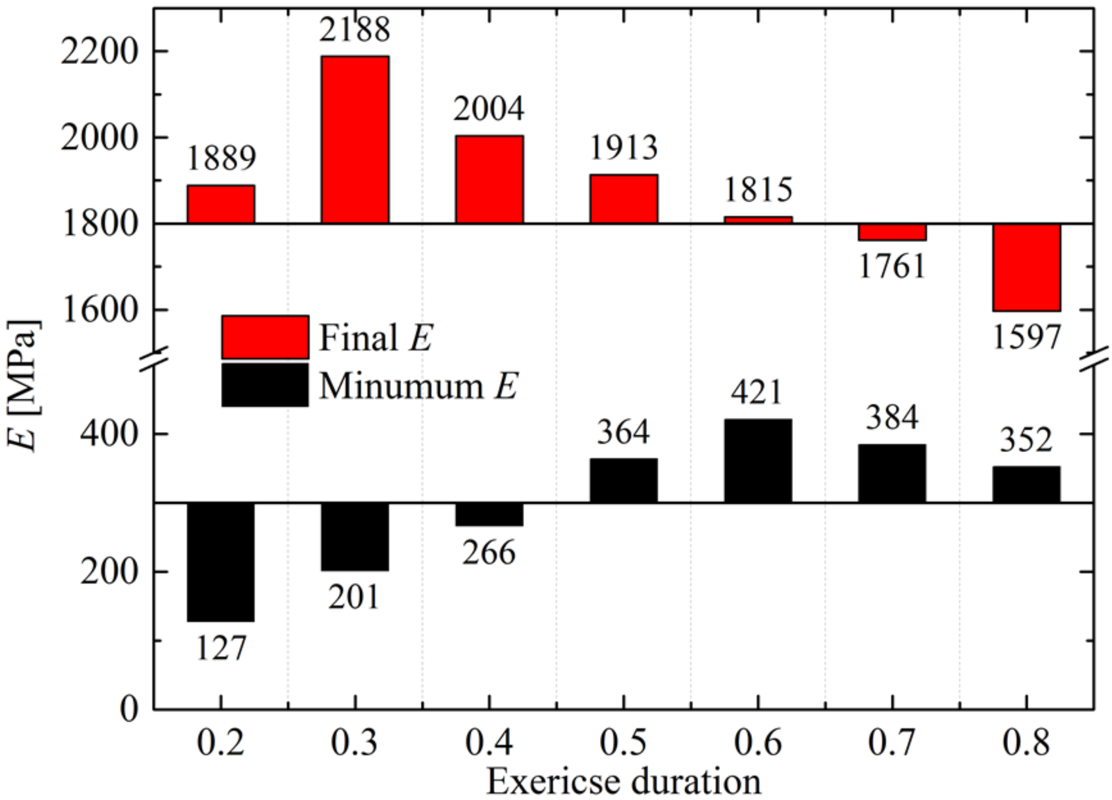

Correct x label